Corrections to facilitate planar imaging of particle concentration in particle-laden flows using Mie scattering, Part 1: Collimated laser sheets

Peter A. M. Kalt,* Cristian H. Birzer, and Graham J. Nathan

University of Adelaide, School of Mechanical Engineering, Adelaide SA 5005, Australia

*Corresponding author: pkalt@mecheng.adelaide.edu.au

Received 23 February 2007; revised 7 June 2007; accepted 11 June 2007;
posted 11 June 2007 (Doc. ID 80305); published 9 August 2007

Planar nephelometry is a laser-based technique of imaging the light scattered from particles to provide information about the local number density of these particles. In many seeded flows of practical interest, such as pulverized coal flames, particle loadings are sufficiently high for the incident laser beam to be severely attenuated. Measurements in these flows are therefore difficult, and limited data are available under these conditions. Laser attenuation experiments were conducted in suspensions of spherical particles in water at various concentrations. This is used to formulate a calibration for the effects of diffuse scattering and laser sheet extinction. A model for the distribution of light through a heavily seeded, light-scattering medium is also developed and is compared with experimental results. It is demonstrated that the scattered signal may be considered proportional to the local particle concentration multiplied by the incident laser power. The incident laser power varies as a function of the attenuation by obscurement. This correction for planar nephelometry images thus extends the technique to provide pseudoquantitative data for instantaneous particle concentration measurements.

OCIS codes: 290.5850, 100.2000, 110.2970.

1. Introduction

There is significant interest in imaging of suspended particles under conditions in which they occupy a sufficient proportion of the fluid volume for their presence to have a nonnegligible influence on optical attenuation. This interest arises both from the many practical applications in which particle loadings are within this regime and from the many advantages offered by planar imaging over single-point measurements. However, the ability to perform such imaging in a quantitative manner is complicated by the effect of the particles, both in attenuating the light source (typically a laser) on its way to the measurement volume, a parameter often termed extinction, and in attenuating the scattered signal on its way to the detector, a parameter typically termed signal trapping. These effects are particularly difficult to account for in turbulent environments where the distribution of particles varies significantly, both in time and space. For these reasons, previous investigations of instantaneous particle number densities have either employed single-point measurements [1] or have been undertaken under conditions for which the effects of attenuation can be neglected [2–4]. The present work seeks to overcome this limitation by developing a method to account for the effects of optical attenuation, at least under conditions of moderate particle loading.

Previous measurements of number density in multiphase flows of density sufficient to cause some attenuation have been performed only by single-point methods. Fan *et al.* [5,6] used a laser diffraction method to measure the particle concentration in the fully merged, self-similar region of coannular jet flows. Fan *et al.* [6] also used used laser Doppler anemometry to determine the velocities of both phases. Using a similar method, Shuen *et al.* [7] measured particle concentrations using isokinetic sam-

0003-6935/07/235823-12$15.00/0

pling and the velocity measurements of both phases. Tsuji *et al.* [8] measured particle concentrations and velocities at a single point by counting pulses from a laser Doppler velocimetry setup, as did Hardalupas *et al.* [1]. For higher mass loadings of particles an optical probe was used to measure the concentration. Similarly Black *et al.* [9] reported the use of phase Doppler particle anemometry to measure the velocity of spherical and nonspherical particles emerging from coaxial and swirling flows. Some planar measurements of particle number density have been performed. However, these measurements have required sufficiently high resolution of sufficiently small areas and the use of sufficiently low particle loadings to allow the counting of individual particles [4,10]. Also worth noting is the laser sheet drop-sizing method introduced by Jermy and Greenhalgh [11] and applied by Zimmer *et al.* [12]. This approach simultaneously measures the concentration and diameters of droplets in a spray using laser-induced fluorescence (LIF) and Mie scattering. Issues of dynamic range limit the range of droplet sizes available to be measured using the drop-sizing method. Also, applying it to solid particles, rather than fluorescent droplets, has technical issues that are presently unresolved. Hence, with currently available approaches, it is not possible to perform reliable planar measurements of particle number density on an instantaneous basis under conditions in which the particle loadings are sufficient to cause significant optical attenuation. Furthermore, this constraint is hampering the development of understanding and models of such flows, which have wide practical significance.

Planar measurements, where they are viable, offer many advantages over single-point measurements in turbulent flows because they provide information about the instantaneous spatial relationships between the measurement volumes. Planar measurements have been critical in advancing the detailed understanding of turbulent flames, such as providing measurements of the structure and thickness of reaction zones (e.g., see [13]). Planar measurements are no less desirable in multiphase flows. This is because the instantaneous distributions of particles are typically highly nonuniform and quite different from their mean values. For example, Longmire and Eaton [4] and Eaton and Fessler [3] have shown that, for low mass loadings, particles exhibit clustering effects. In turbulent shear flows, particles tend to congregate preferentially in instantaneous regions of high strain and low vorticity. Similarly, Smith *et al.* [10,14] found that the presence of such instantaneous nonuniform distributions of fuel particles can have a significant effect on the combustion of pulverized fuel flames.

Earlier attempts have been made to quantify the role of attenuation and signal trapping in some select applications. Laser diagnostics of conical sprays has motivated much of this early work, and many preliminary and key papers appear in the proceedings of technical conferences rather than the archival literature. Great success has been demonstrated in correcting attenuation and signal trapping in conical sprays because the degree of axial symmetry enables out-of-plane information to be well inferred from in-plane information [15–18]. This approach is limited in more complex cases with less instantaneous axisymmetry.

One such method uses counterpropagating laser sheets to image data in both the forward- and backward-scattering modes [15,18–20]. If the temporal separation between the counterpropagating laser sheets is small enough, then it can be assumed that the flow is frozen and differences in the two images are due to attenuation of each laser light sheet only. The underlying assumption is that only the laser sheet is attenuated, proportionally reducing the generated signal, and that there is no trapping of the signal. A numerical procedure based on the Beer–Lambert law is used to recover the true intensity distribution from the counterpropagating images, either from the simple average of the two images [19] or the ratio of the images.

Koh *et al.* [15] use another method based on the Beer–Lambert absorption within a conical spray. The Beer–Lambert corrections require a path length and attenuation coefficient for each pixel. In this study, these values were found using counterpropagating laser sheets and two cameras to build a set of attenuation coefficients and path lengths for a specific spray-cone geometry. They find that attenuation affects both the LIF and Mie signal in a similar way, which is a positive outcome for planar Mie and LIF drop-sizing methods since attenuation errors on each signal should largely compensate each other.

Jermy *et al.* [16,17] used a Monte Carlo simulation of particles to pick apart the role of multiple scattering events through a densely seeded conical spray. Such sprays are sufficiently attenuated to cause most detected photons to have undergone multiple scattering events. In that study attenuation is estimated by uniformly backlighting the flow to determine mean overall attenuation. The simulations provide reasonable agreement with experimental estimates. They also enable an estimation of uncertainties due to attenuation and photon scattering, which will affect signal trapping.

Sick *et al.* [18] examined a hollow cone spray and considered the effects of attenuation on both the planar LIF and Mie signals for the planar drop-sizing technique. Trapping of the signal was also considered. Again, this approach requires rotational symmetry of the hollow spray cone and so is not applicable to asymmetrical distributions of particles.

Hertz and Alden [21] have developed an iterative correction applied to 1-D OH LIF measurements. If the spatially resolved measurement of OH is measured and the absolute attenuation across the measurement is known, then the Beer–Lambert law can be applied by iteration. The advantage of this method compared with counterpropagating methods is that no spatial information is required and no assumptions need to be made regarding the distribution of the fluorescing medium. However, it has not been extended to 2-D imaging.

Abu-Gharieb *et al.* [22] also demonstrate the feasibility of an iterative approach to compensating for laser sheet attenuation in a planar Mie scattering image. In that study, a correction for attenuation based on a monodisperse solution of particles in water is determined that can then be applied to flows of similar particles through the same detector. That method is not generally quantifiable until the Mie signal generated by a particle can be related to the Beer–Lambert absorption caused by that particle.

There remains a need for improved planar measurement capabilities in heavily seeded two-phase flows. The present paper aims to address this need and develop a correction for the effects of attenuation on a shot-by-shot basis. The correction for attenuation should be general enough to be applied to flows for which little is known a priori about the distribution of particles or the structure of the flow. This approach is necessary because of the significant differences between the mean and instantaneous distributions in turbulent systems. The present study is limited to collimated light sheets; however, it is derived in such a way that the simplified 1-D derivation is extendable to 2-D (or even 3-D) imaging applications. The application to diverging light sheets is dealt with in the accompanying paper [23].

2. Laser Sheet Extinction

A. Beer–Lambert Absorption

The Beer–Lambert law [24,25] is a description of the relationship between the absorption of light and the properties of the medium through which it moves, as shown in Fig. 1. The transmittance, I_1/I_0, refers to the ratio of light leaving the medium, I_1, related to the amount of incident light, I_0. By considering an axis along the path of the light, x, the medium can be considered to be the concatenation of a series of infinitely thin slices along the x axis. These slices have an area perpendicular to the direction of light, A_{slice}. Similarly, a single scattering body has a cross-sectional area perpendicular to the path of the light. In nephelometry, the scattering bodies are spherical particles, so the area of the particle shadow is $A_p = \pi r_p^2$. This shadow is small compared with the area of the slice. The opaque fraction of a single particle is given by $\Upsilon_1 = A_p/A_{slice}$. The transparent fraction, $\Gamma_1 = 1 - \Upsilon_1$, is the amount of light transmitted past a single scattering body.

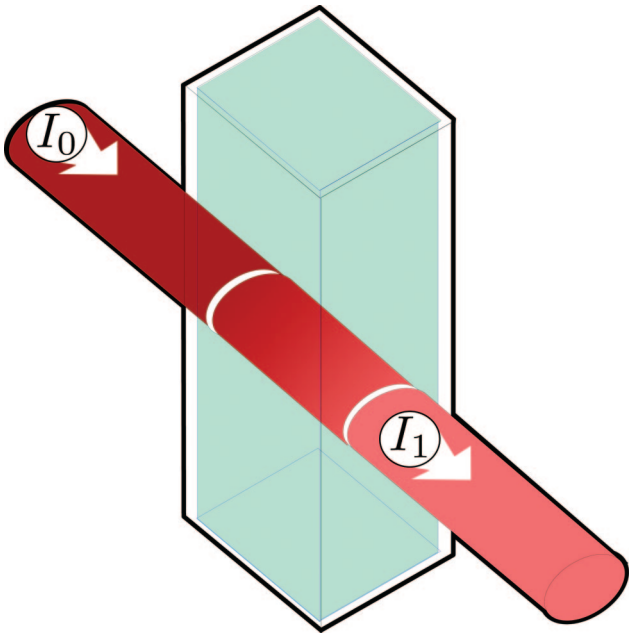

Fig. 1. (Color online) Light beam passing through an absorbing medium.

Next we consider the effects of multiple scattering bodies. The Beer–Lambert formulation assumes that particle shadows do not overlap and is only accurate at low dilutions, i.e., with a transmittance greater than 90%. In this case, multiple particles simply add to the opaque area, so for n_p particles in a slice, the opaque fraction becomes $\Upsilon_{n_p} = (n_p A_p)/A_{slice} = n_p \Upsilon_1$. The fraction of photons absorbed when passing through a slice is equal to the total opaque fraction, determined as the ratio of the opaque bodies projected area to the total projected area:

$$\frac{dI_x}{I_x} = \frac{A_p n_p}{A_{slice}} = \frac{A_p (A_{slice} dx) c}{A_{slice}} = -A_p c dx. \tag{1}$$

The particle concentration, c, is directly related to the number of particles in a given volume. The number of particles in the slice is equal to $n_p = cV = c(A_{slice}dx)$. The transmittance over a path length, l, through the medium is found by integrating with respect to x to give

$$\frac{I_1}{I_0} = \exp(-A_p l c). \tag{2}$$

This is the well-known Beer–Lambert law,

$$\frac{I_1}{I_0} = 10^{-\alpha l c}, \tag{3}$$

where $\alpha = A_p/\ln 10$.

B. Extinction of a Collimated Beam by Particles

Kalt and Birzer [26] introduced a formulation of a ray-based extinction of light by overlapping particles, which is presented in more detail here. Consider the ray tracing of shadows through a two-phase medium for the case of a collimated light sheet, as shown in Fig. 2. The laser sheet can be considered to be an illuminated volume of fixed cross section for this case. The height and width of the beam, δy and δz, are independent of location down beam.

As a particle enters this volume, it will elastically scatter light as described by the generalized Lorenz–Mie theory [27]. If the particle is large relative to the wavelength ($d_p \gg \lambda$), then the scattering is proportional to the projected area of the particle, πr_p^2. Each

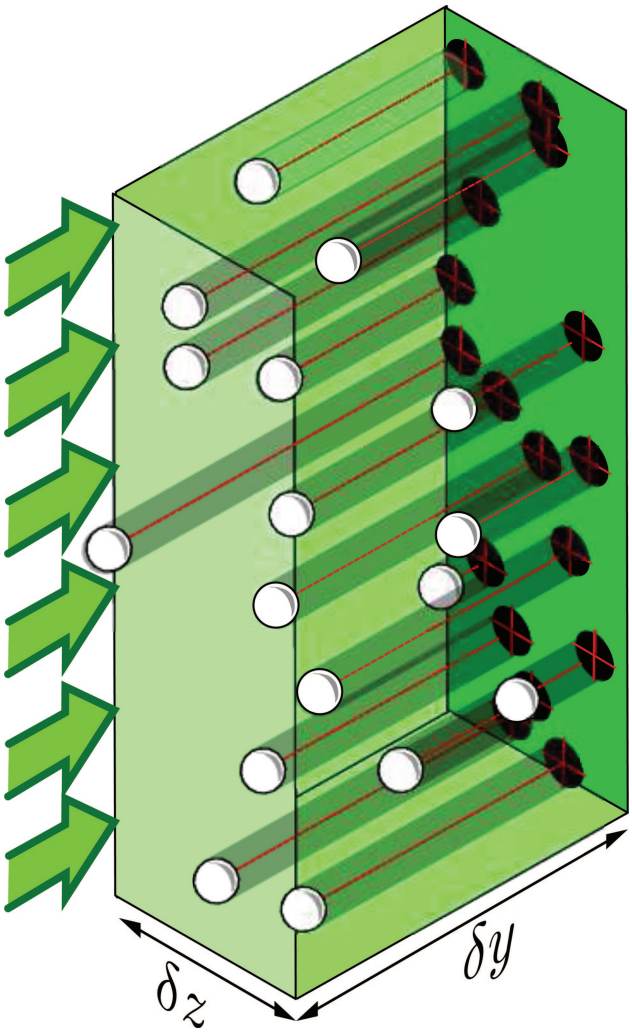

Fig. 2. (Color online) Schematic representation of the cylindrical (and potentially overlapping) shadows cast by spherical particles for the case of collimated light.

particle also casts a cylindrical shadow that persists down beam, indefinitely if we neglect diffraction.

The transmitted fraction of the light remains to interact with subsequent scattering bodies. If the particles are small relative to the laser cross-sectional area, then the transmittance can be considered as the probability of photons passing n_p scattering bodies. If the transparent fraction of a single particle is Γ_1, then the transmittance over a path l, which contains n_p particles, is

$$\frac{I_1}{I_0} = \Gamma_1^{n_p} = (1 - A_p/A_{slice})^{n_p}. \tag{4}$$

It is easy enough to use the product identity

$$\prod_{i=1}^{\infty} f_i = \exp\left(\sum_{i=0}^{\infty} \ln f_i\right) \tag{5}$$

to express the transmittance in a more familiar form, namely,

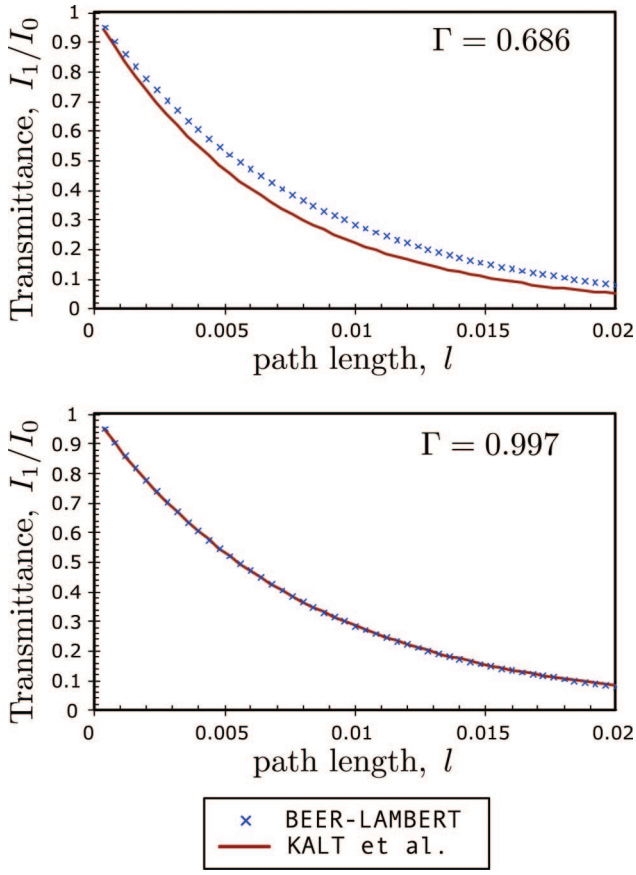

Fig. 3. (Color online) Behavior of the extinction models for different particle sizes.

$$\frac{I_1}{I_0} = \prod_{}^{n_p} \Gamma_1 = \exp(n_p \ln \Gamma). \tag{6}$$

These two descriptions for the absorption and transmittance are identical if there are no particle shadows overlapping, i.e., for very small particles or very dilute concentrations. When the concentration increases or particles are large compared with the area of the slice, then shadows will start to overlap with increasing probability. In this scenario, the Beer–Lambert formulation will overpredict the transmittance because nonovelapping shadows will increase the shadow area. Figure 3 shows the similarity of the two models at low and high transparent fractions and concentrations.

C. Scattered Signal

Early work on the Mie signal scattered by particles has been done by Becker *et al.* [28] and others. Becker *et al.* assessed the use of a broad-spectrum light source and tiny particles as flow tracers with a view to derive the turbulence statistics of the underlying fluid flow. They describe the proportion of the light that is detected as a Mie-scattered signal, based on the parameters describing the illumination, optics, detection, and particle properties. Becker's general formulation is given as

$$\int_0^\infty \Phi_K d\lambda = \pi r_p^{\,2} n_p \omega_i \omega_s \int_0^\infty \psi_{av} \tau_L \tau_1 \tau_i \tau_s \tau_2 \tau_p I_0 d\lambda. \quad (7)$$

Readers are encouraged to refer to the original reference for details, but in summary, Φ is the detected signal, τ are the transfer efficiencies of the signal through stages of detection, ω_i and ω_s are the solid angles of illumination and collection, ψ_{av} is the Mie-scattering cross section, and I_0 is the incident illumination.

For the current study, the planar laser technique allows substantial simplifications to Eq. (7). First, the use of a monochromatic source eliminates dependencies on the wavelength λ. Second, influences of the illumination strength can be grouped together with incident laser power into a local laser intensity, I', where the prime superscript is used to denote the local quantity. Finally, the proportional constants representing Mie scattering and collection efficiencies can be grouped together into a single constant, C_κ. The signal onto the detector is comprised of a signal from particles Φ_p and a background signal Φ_{bkg}, contributed from detector noise, ambient light, and diffuse scatter, i.e.,

$$\Phi = \Phi_p + \Phi_{bkg}. \quad (8)$$

The signal from particles can be more simply expressed as

$$\Phi_p = \overline{\pi r_p^{\,2}} C_\kappa n_p I', \quad (9)$$

where $\overline{\pi r_p^{\,2}}$ is the average particle cross-sectional area available to scatter the signal and n_p is the number of scattering bodies. I' is the local, corrected intensity of the laser sheet adjusted for losses, including laser sheet extinction and divergence where applicable. C_κ represents an overall scaling constant, accounting for collection optics and particle scattering efficiency.

Provided that the optics, magnification, and particles are kept constant, then C_κ should not change. In practice C_κ may vary slightly over the entire imaged region because of optical variations over the image. On the detection side, C_κ is influenced by the detection optics, magnification, and f#. Provided that the optics are selected appropriately, it should be possible to avoid vignetting and other variations of the signal throughput across the imaged area. The imaging of a uniform light source is an appropriate experimental validation to enable confirmation of the consistency of C_κ across the image. This variation due to optics is able to be neglected for most imaging applications where the solid angle is kept small (i.e., small aperture and high f#).

On the signal side, C_κ is dependent on the particle size and shape, as well as the Mie-scattering cross section, which is dependent on temperature. The technique is limited to conditions where these experimental variables are consistent and known. The scattered signal, Φ_p, is also mildly affected by the scattering angle. If a large region is imaged, then the scattering angle for Mie scattering may differ enough between the up-beam and down-beam edges of the image to affect C_κ up to 10%. Increasing the distance between the camera and the imaging plane serves to reduce the parallax discrepancy and make C_κ independent of scattering angle. The value of C_κ needs to be determined accurately for a given condition, a method that is described in Subsection 5.A.

D. Raster Imaging Plane

In digital planar imaging methods, data are recorded by a CCD detector, which contains a 2-D array of pixels. By selecting the collection optics magnification, the signal on the CCD (the image plane) corresponds to a region of space illuminated by the laser sheet (the object plane). If the CCD is an $n \times m$ array of pixels, and each pixel corresponds to an in-plane resolution ($\partial x = \partial y = R$ μm/pixel), then the imaging region is nR μm $\times$ mR μm. Figure 4(a) shows the imaging region, located within the laser sheet. The signal from the entire pixel volume contributes to a single discrete value stored in the pixel. This digital representation is known as a raster.

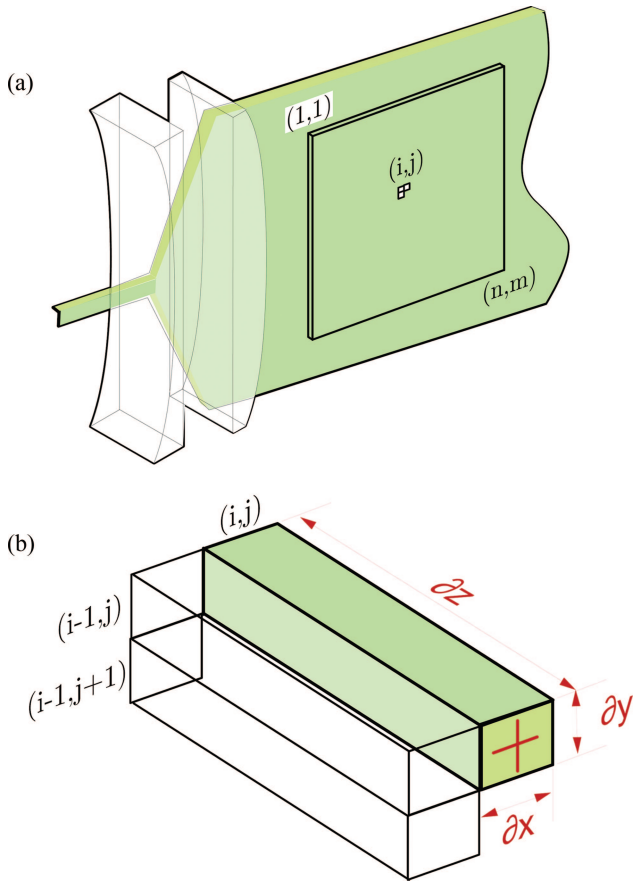

Fig. 4. (Color online) (a) Imaged plane of an $n \times m$ CCD. (b) Imaged pixel volume; ∂x and ∂y are in-plane resolution, ∂z is laser sheet thickness.

The correction for attenuation needs to be implemented for the rasterized Mie-scattering images. The origin of the raster plane is defined to be at the top left of the image. The region of space imaged by each pixel on the CCD detector corresponds to a pixel volume in the shape of an extruded prism, with a height, ∂x, and width, ∂y, corresponding to the in-plane resolution of the camera, and a depth, ∂z, equivalent to the thickness of the laser sheet. This is shown schematically in Fig. 4(b). In the present paper the corrections are derived for a collimated laser sheet that is aligned to the orientation of the raster. In the second part of this study [23], the formulation is extended to diverging sheets in which the orientation of the laser sheet is not always aligned with the raster plane.

When Eq. (9) is expressed in terms of rastered pixel volumes, the signal of a pixel located at $[i, j]$ is

$$\Phi_p[i, j] = C_\kappa\left(\overline{\pi r_p^2}\right) n_p[i, j] I'[i, j], \tag{10}$$

where $n_p[i, j]$ is the number of particles in the pixel volume at $[i, j]$ and $I'[i, j]$ is the incident laser power entering the pixel located at $[i, j]$. For clarity, if a quantity varies spatially across an image we will omit the indices of the raster plane pixel position $[i, j]$ and denote the quantity with a tilde. Equation (10) may then be more succinctly expressed as

$$\tilde{\mathbf{\Phi}}_\mathbf{p} = C_\kappa\left(\overline{\pi r_p^2}\right) \tilde{\mathbf{n}}_\mathbf{p} \tilde{I}'. \tag{11}$$

Implementation of the corrections for attenuation is readily implemented on a per-pixel basis. Referring to the derivation of the ray-based formulation for extinction of the laser sheet in Subsection 2.B, the rays can be analyzed as a row of pixel volumes. The amount of light unaffected by particle scatter in each pixel volume is the transmittance across the pixel volume,

$$\tilde{\kappa}_{trans} = \left(1 - \frac{\overline{\pi r_p^2}}{\partial x \partial z}\right)^{\tilde{\mathbf{n}}_\mathbf{p}}, \tag{12}$$

where the laser sheet area is now replaced by the down-beam surface area of the pixel volume. The absorption coefficient, $\tilde{\kappa}_{trans}$, now represents the fraction of the light transmitted through a pixel volume.

3. Experimental Validation

To test the validity of the extinction and scattering formulations, planar nephelometry measurements were made in various known and homogeneous suspensions of solid spherical particles in water. Figure 5 shows a schematic diagram of the experimental rig. Various quantities (0.0 to 3.0 g in 0.2 g increments) of polyamid spherical particles (PSP-20) with a mean particle diameter of 20 μm and a density close to water ($\delta = 1.030$) were suspended in a 20 l Perspex tank designed for water visualizations. This corresponds to a series of volume fractions, F_V, ranging from 0 to 97.1 parts in 10^6 (ppm) in increments of 9.71 ppm. The 20 μm particle size was selected as being typical of particles in pulverized fuel and spray combustion systems. The volume is intermittently stirred to maintain homogeneous particle distribution.

A collimated laser sheet is created from a Nd:YAG laser, using the second-harmonic output of 532 nm at low power (20 mJ/pulse). This beam is formed by optics into a laser sheet that is 2 mm wide and 27 mm high and is collimated down beam from the final lens. The given arrangement creates conditions analogous to those shown schematically in Fig. 2. The laser sheet is directed through the side wall of the tank. A Kodak Megaplus ES1.0 camera with a Tamron

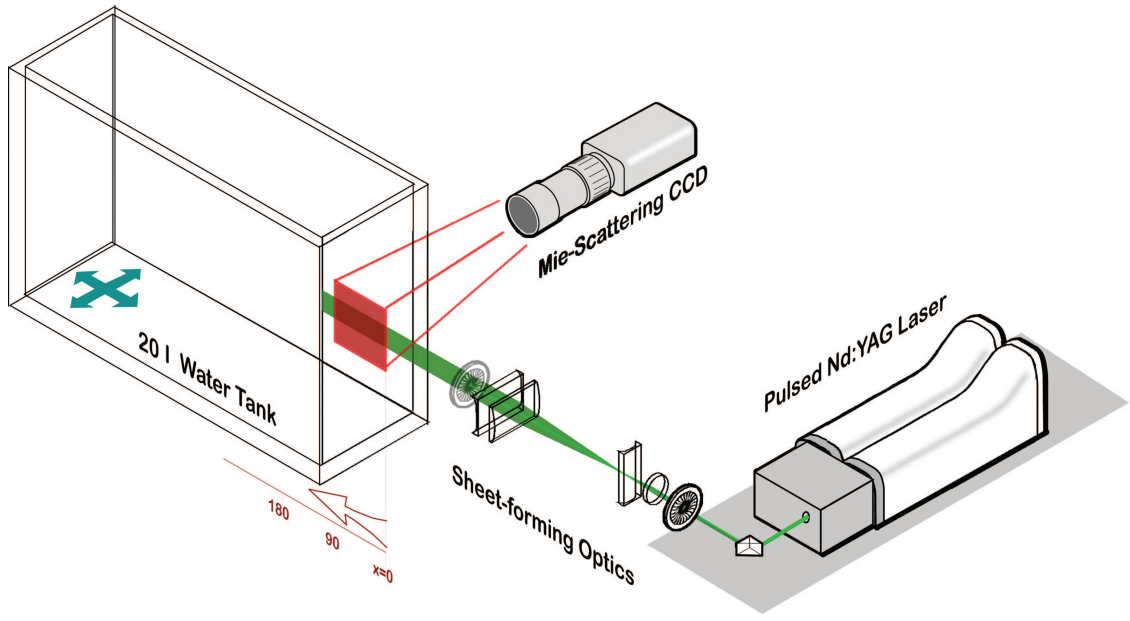

Fig. 5. (Color online) Calibration setup showing tank, laser, and camera.

30–80 mm lens (*f*# 5.6) was used to image a region of 80 mm × 80 mm. Measurements in different regions of the tank were performed by traversing the tank without modifying the camera or laser optics. Translating the tank axially allows path lengths through the medium to be varied. Translating the tank out of plane allows the amount of medium available to contribute to signal trapping to be controlled.

4. Results

For each particle loading and each location, the scattered signal was determined from an ensemble of 100 images. In each case, the ensemble was Gaussian smoothed (3 × 3) and corrected for laser profile and detector background to provide an averaged scattering image. Figure 6 shows a composite of the averaged beam for some selected cases. The intensity increases with concentration of particles, but the response becomes increasingly nonlinear. Detector saturation must also be taken into account in determining the average values, and there is often a tradeoff between sensitivity to signal versus dynamic range of the detector. The average intensity was taken from the integration along a 27 mm high (vertical) column, representing the laser sheet cross section, at each location across the image. These average values are plotted against down-beam distance for each particle concentration case, shown in Fig. 7. Signal-trapping effects are minimized by limiting the out-of-plane thickness of the scattering medium to 5 mm by imaging the beam at the near face of the tank. The solid curves indicate the expected signal calculated for the given PSP-20 particles at the equivalent concentrations by Eqs. (4) and (9), using $C_\kappa = 1.9$.

Furthermore, the local admission fraction can be easily determined for two-phase flows of spherical particles or droplets. Correcting the recorded signal to account for a laser intensity that varies due to transmittance enables the particle loading to be inferred from the signal. Figure 8 shows the results of such a correction applied to the average nephelometry images to account for the transmittance, I'/I_0. The measurement certainty becomes less for cases

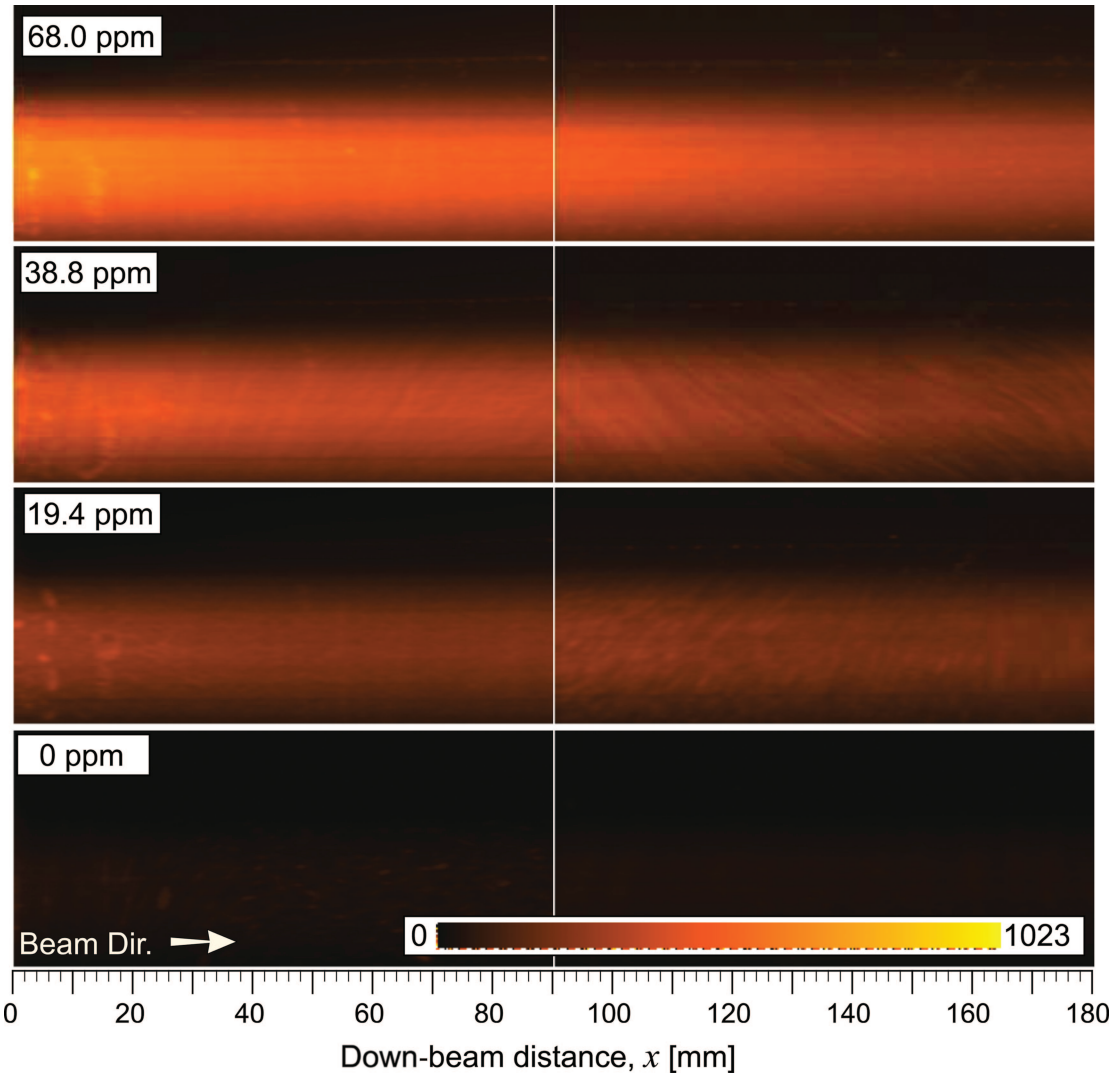

Fig. 6. (Color online) Selected averaged beam images from PSP-20 seeded water tank.

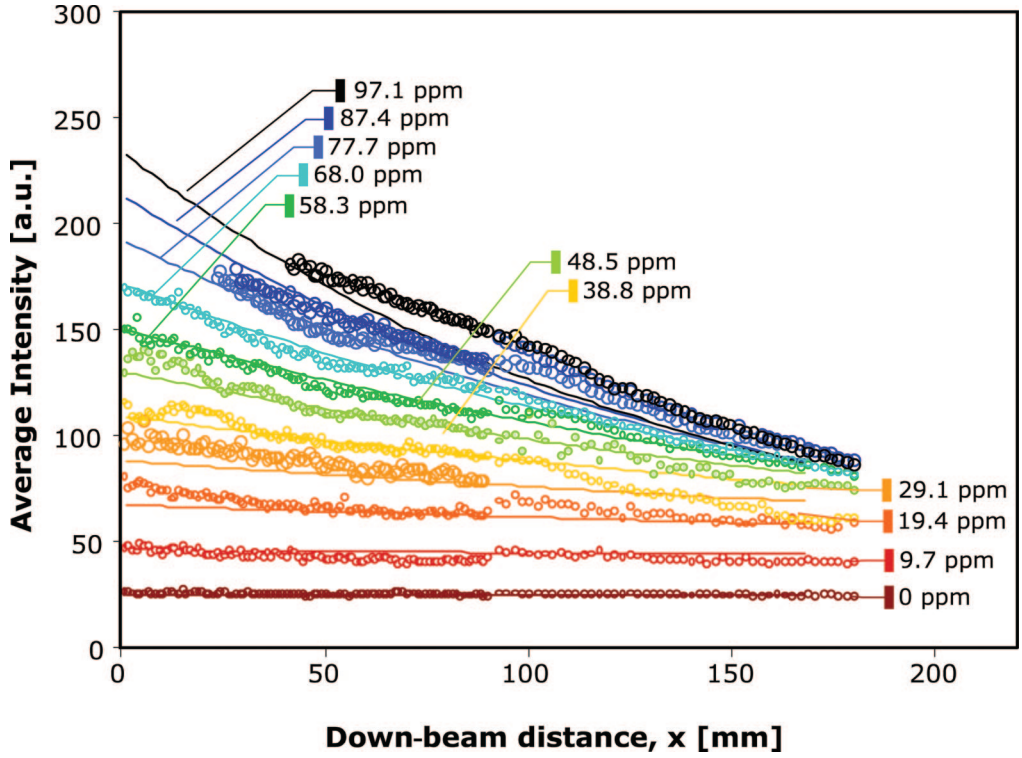

Fig. 7. (Color online) Average signal intensity as a function of extinction path length for PSP-20 particles suspended in water.

where I'/I_0 is low and the normalization for a low local laser power magnifies other errors. Nevertheless, the noise increases as the particle loading increases, in part because saturation of the CCD becomes significant at these cases. However, even at moderate levels, the signal can be corrected and is constant for the entire length of the laser sheet through the tank.

The effect of signal trapping is also assessed by varying the out-of-plane thickness of the scattering medium between the laser sheet and the camera. This is done by translating the tank in the out-of-plane direction. Figure 9 shows how the signal trapping increases, as the out-of-plane thickness is increased from 5 to 75 mm, for a laser sheet entering into a 150 ppm mixture of PSP-20 particles. Also, the signal background, Φ_{bkg}, is seen to increase as the out-of-plane thickness is increased. This signal background is estimated from the detected signal just outside the laser sheet but still in the imaging plane.

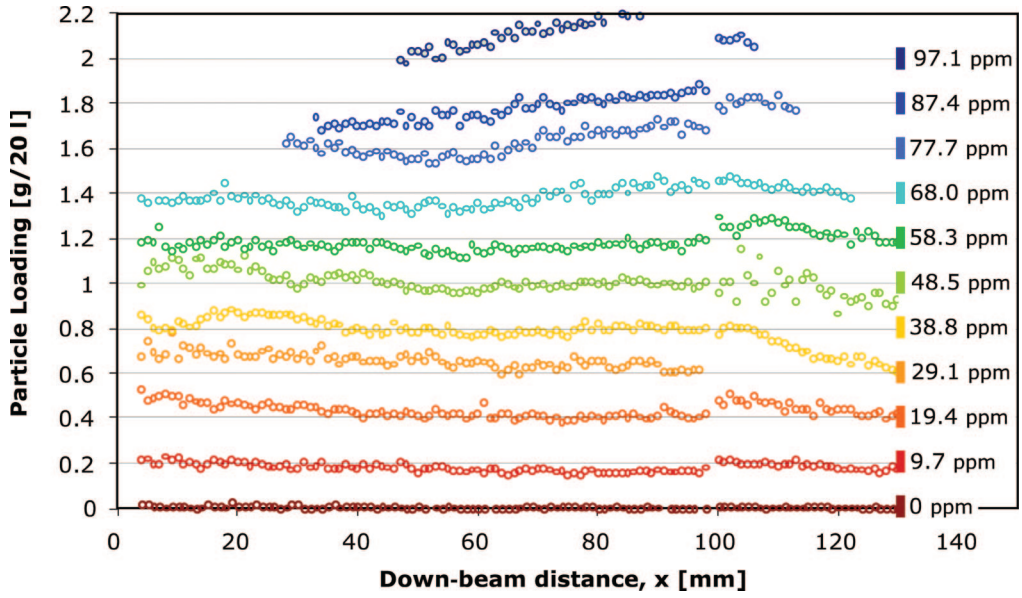

Fig. 8. (Color online) Average intensity corrected for transmittance and normalized for particle loading.

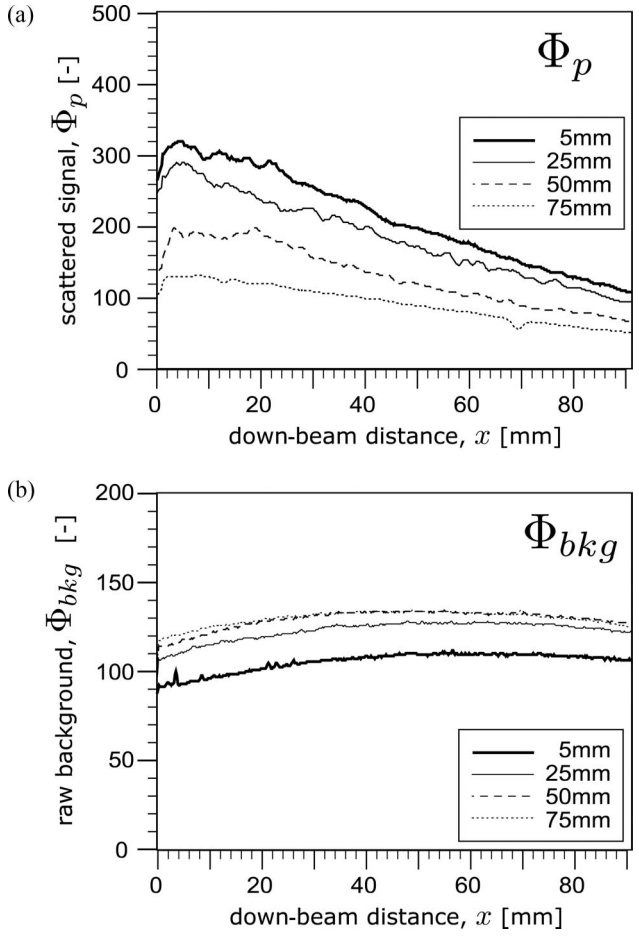

Fig. 9. Signal intensity for 150 ppm medium laser extinction for different out-of-plane depths l_z.

This is attributed to multiple (depolarizing) scattering events, generating diffuse light. The background is contributed from scattering of this diffuse light from particles in the volume of the medium imaged by the camera but not lying within the laser sheet.

5. Discussion

A. Determination of C_κ

There are a number of strategies that can be employed to determine the appropriate value of C_κ if the experiment is set up to facilitate that process. For instance, it is possible to place a reflective polymer strip in the down-beam edge of the imaging region. The laser hitting the sheet will be reflected back into the camera, proportional to the total transmitted laser power per unit area along the laser sheet height. Normalizing the shot-to-shot signal from this strip, by the mean signal without particles, will give an instantaneous record of the transmittance, I'/I_0. A single value of C_κ can be selected that will duplicate the attenuation behavior.

Alternately, a C_κ can be determined by iterating to remove eccentricities in the ensemble mean image of a symmetrical flow. This is often the case when collected data are affected by attenuation of the laser sheet, but the magnitude of attenuation is small enough to disguise the effect when observing the instantaneous data. In such cases, the biases due to attenuation are often only clearly visible in the mean and rms images of particle concentration. If the flow is known to be symmetrical about an axis orthogonal to the light sheet, then C_κ can be selected to remove the bias in the ensemble mean image. The rms image is particularly sensitive to small fluctuating quantities.

Finally, C_κ can be selected to match the known particle concentration in a calibrated flow, as is used in Section 3 in this study to match the scattered signal to a known concentration. A value of C_κ determined in this way will be applicable to other experimental configurations provided that the particles, optics, and laser power remain unchanged. It is therefore useful to calibrate the signal detection to a known concentration of the investigated particles. Such a strategy will allow the planar nephelometry images to be postprocessed to provide quantitative particle concentration measurements, provided that attenuation does not completely extinguish the probe beam (i.e., laser sheet).

B. Heterogeneous Particle Distributions

At any given pixel in the imaged region, the local laser intensity, $\tilde{I}'$, will need to account for the history of extinction (attenuation by particles). These effects are cumulative along the beam path. When considering the effects of attenuation by particles along a collimated 1-D beam, the local laser intensity at the nth element is expressed as

$$\tilde{I}_n' = \left(\prod_{i=1}^{n} \Gamma^{n_p[i]}\right) I_0 \tag{13}$$

$$= \kappa_{atten}[n]\tilde{I}_{n-1}'. \tag{14}$$

The number of particles located in any given pixel volume must be determined to find κ_{atten}. In a homogeneous seeded medium, the number of particles, n_p, is known from the concentration. If the concentration is not known *a priori* or the local concentration varies in a heterogeneous mixture, then n_p can be found using Eq. (11) provided that the scattering coefficient, C_κ, is known or can be estimated. It is then possible to combine the effects of extinction along the whole of the beam by recursion, using a value of $\tilde{I}_{n-1}'$ taken from the pixel immediately down beam of our pixel at $[i, j]$. This can be done by assuming that the contribution to extinction within any single individual pixel is small and the term $\tilde{I}'$ [in Eq. (11)] is equal to the amount of light entering the pixel, namely, $\tilde{I}_{n-1}'$.

C. Effect of Signal Trapping

The effects of signal trapping can be reduced if the solid angle of the collection optics is large enough and the CCD is far enough away from the imaging plane for the difference in scattering angle between the two

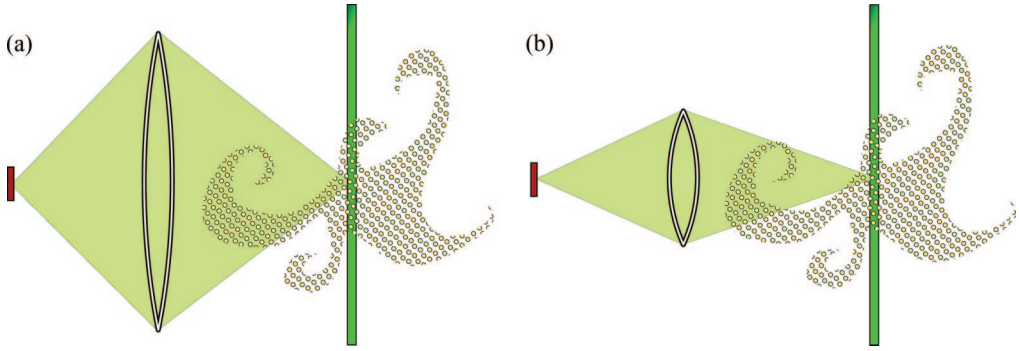

Fig. 10. (Color online) Schematic of the effect of the size of collection optics on signal trapping.

sides of the image to be neglected. Large-aperture optics also reduce the significance of signal trapping by making the magnitude of the trapping more dependent on mean mass loading (which is measurable) and less dependent on local position and out-of-plane inhomogeneities in the particle distribution (which are unknown and not easily measured). This is illustrated schematically in Fig. 10. Note that the case presented is highly idealized. Furthermore, in reality large aperture optics will result in increasingly nonuniform response over the image, meaning that C_κ is no longer constant over the imaged region. It is therefore advantageous to optimize the uniformity of the detector response (consistent C_κ over an image) and to use strategies based on the in-plane measurements to correct signal trapping.

Trapping of the scattered signal between the laser sheet and camera is analogous to the extinction of the beam through the scattering medium. In Fig. 11, the recorded signals from various out-of-plane path lengths, l_z, presented in Fig. 9 are adjusted for the transmittance of light through a path length equal to the out-of-plane distance. The transmittance for the various path lengths are found using Eq. (6) for the case of $F_V = 150$ ppm. The normalized signals are presented in Fig. 11.

The extinction model corrections perform very well when applied to signal trapping in the homogeneous medium. In the down-beam regions ($x > 40$) the corrections are accurate to within 5%–10%, which is within the limits of other experimental errors. In the up-beam regions ($x < 30$) the signal is adversely influenced by the saturation of the detector, since the raw signal at such heavy particle loading ($F_V = 150$ ppm) was not optimized for the detector dynamic range in this region. These results confirm that the extinction model is useful to define error bars for measurements where signal trapping occurs. Furthermore, the extinction model can be used to correct for mean signal trapping effects on an ensemble mean and rms image of particle concentration, provided the flow is axisymmetrical and in-plane structure can be used to infer out-of-plane distributions of particles contributing to signal trapping. Correcting for signal trapping in this way reduces signal-trapping errors from approximately 50% to 5%–10% depending on the degree of attenuation.

D. Error Analysis

The estimated errors for an axisymmetric particle-laden flow are calculated and presented in Fig. 12 as

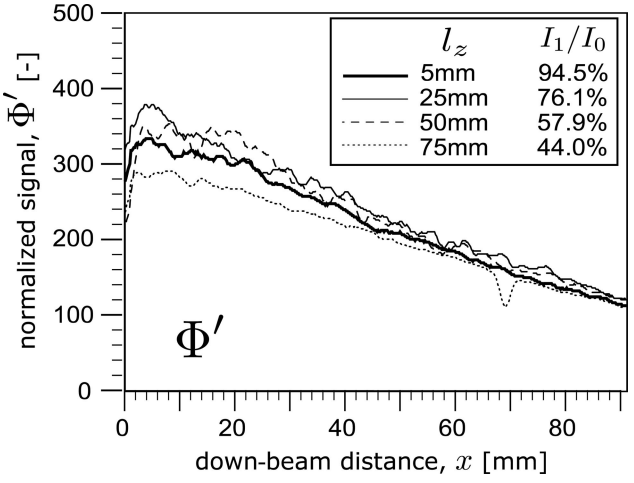

Fig. 11. Normalized signal ($F_V = 150$ ppm) using extinction model corrections for signal trapping.

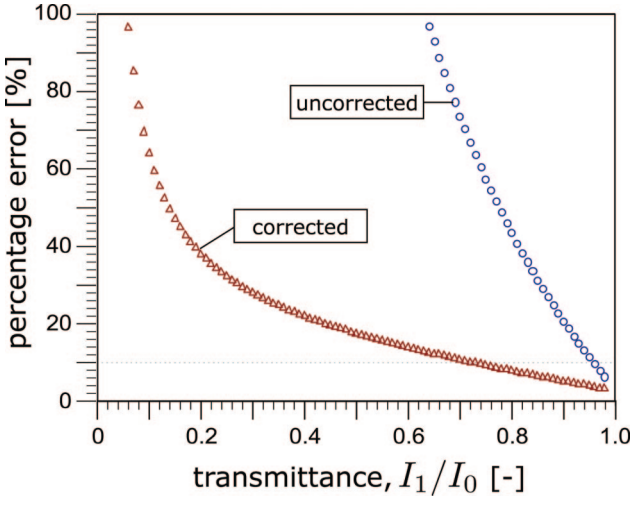

Fig. 12. (Color online) Relative certainty of measurements as a function of the transmittance I_1/I_0 for a 10 bit detector.

a function of overall transmittance, I_1/I_0. The transmittance is an appropriate parameter describing the effect of attenuation, since it is easily determined experimentally and applies equally to both homogeneous and heterogeneous distributions of particles. The effect of signal trapping is estimated for an axisymmetric flow where the distribution of particles out of plane is radially similar to the mean distribution resolved in plane. The detector noise and dynamic range for a 10 bit camera are estimated, with the dynamic range optimized to avoid saturation in the instantaneous images. In the case of almost no saturation ($I_1/I_0 = 1$), the signal-to-noise ratio of the data is usually approximately 100, and the measurement errors are as low as 1%. The errors become enormous quickly if the effect of attenuation is not accounted for, since the trapping suppresses the signal simultaneously by attenuating the incident laser power and trapping the scattered signal on the way to the detector. However, estimation of the transmittance can be achieved to within 5%–10%, as can the effect of signal trapping. At very high transmittances ($I_1/I_0 \rightarrow 1$) these errors are approximately 1%. In any case, even when corrected the errors are able to be reduced to approximately 10% for transmittances down to 60%, i.e., $0.6 < I_1/I_0 \leq 1$. This greatly expands the range of particle loadings where quantifiable measurements are now able to be performed in particle-laden flows. When the effects of attenuation are beyond this limit, the data accuracy suffers because the effective dynamic range of the detector is reduced as the signal is attenuated and approaches the detector noise.

6. Conclusions

A planar nephelometry technique has been developed to facilitate quantitative measurements of the particle concentration in two-phase flows at substantially higher mass loadings than was previously possible. The technique requires the formulation of a model to account for the extinction of a collimated laser sheet by particles. A ray-based model that neglects diffraction is presented (based on the Beer–Lambert Law of gaseous absorption) to determine the transmittance through a seeded medium. Additionally, a simple linear scaling relationship relates the detected signal to the number density of particles through a scaling parameter, C_κ, that accounts for the optics and the particle scattering properties. The validity of the attenuation and scattering models was tested experimentally. Mie-scatter images using a collimated light sheet were collected in various homogeneous mixtures of particles of known size and concentration. A constant, single value of the scaling parameter, $C_\kappa = 1.9$, was found to allow the concentration to be determined to within 3% in most cases and not worse than 10%, even at the highest particle loadings ($F_V \sim 100$ ppm). It should be noted that in this case, the incident laser light is reduced by up to 50% because of attenuation due to particles, over a path length of 150 mm. Uncorrected, this is an error that prevents all but the most basic, qualitative analysis of the images. The performance of the models is exceptionally good, and correction for attenuation allows measurements of particle concentrations to be accurate to within other experimental uncertainties.

Another benefit of the formulation presented here is that it is readily implemented in heterogeneous particle mixtures, such as two-phase mixing problems. This is because the extinction of the laser sheet at any given point is based on the extinction history along the ray up to that point. In a heterogeneous flow, the extinction history may be found from the number of particles along the beam, and the number of particles can be found from the signal by applying the scattering model.

The formulation given in this study is derived for 1-D attenuation along a collimated beam, aligned to the raster plane of the image. In practice, this limits the imaged region height to the size of the sheet-forming optics, typically 50 mm. This scale, though useful to reveal small-scale mixing in industrial-scale problems, is insufficient to resolve macroscopic phenomena, such as roping and clustering, known to occur in large-scale particle-laden flows. The extension of the present 1-D formulation to diverging sheets and its validation in imaging large-scale two-phase mixing problems forms the companion paper [23].

This work has been supported by the Turbulence, Energy and Combustion Group at the University of Adelaide and by the Australian Research Council.

References

1. Y. Hardalupas, A. M. K. P. Taylor, and J. H. Whitelaw, "Velocity and particle-flux characteristics of turbulent particle-laden jets," Proc. R. Soc. London **426,** 31–78 (1989).
2. J. R. Fessler, J. D. Kulick, and J. K. Eaton, "Preferential concentration of heavy particles in a turbulent channel flow," Phys. Fluids **6,** 3742–3749 (1994).
3. J. K. Eaton and J. R. Fessler, "Preferential concentration of particls by turbulence," Int. J. Multiphase Flows **20,** 169–209 (1994).
4. E. K. Longmire and J. R. Eaton, "Structure of a particle-laden round jet," J. Fluid Mech. **236,** 217–257 (1992).
5. J. Fan, H. Zhao, and K. Cen, "An experimental study of two-phase turbulent coaxial jets," Exp. Fluids **13,** 279–287 (1992).
6. J. Fan, H. Zhao, and K. Cen, "Particle concentration and size measurements in two-phase turbulent coaxial jets measurements in two-phase turbulent coaxial jets," Chem. Eng. Commun. **156,** 115–129 (1996).
7. J.-S. Shuen, A. S. P. Solomon, Q.-F. Zhang, and G. M. Faeth, "Structure of particle-laden jets: measurements and predictions," AIAA J. **23,** 396–404 (1985).
8. Y. Tsuji, Y. Morikawa, T. Tanaka, and K. Karimine, "Measurement of an axisymmetric jet laden with coarse particles," Int. J. Multiphase Flows **14,** 565–574 (1988).
9. D. L. Black, M. Q. McQuay, and M. P. Bonin, "Laser-based techniques for particle-size measurement: a review of sizing methods and their industrial applications," Prog. Energy Combust. Sci. **22,** 267–306 (1996).
10. N. L. Smith, "The influence of the spectrum of jet turbulence on the stability, nox emissions and heat release profile of pulverised coal flames," Ph.D. thesis (University of Adelaide, 2000).
11. M. C. Jermy and D. A. Greenhalgh, "Planar dropsizing by elastic and fluorescence scattering in sprays too dense for

phase doppler measurement," Appl. Phys. B **71,** 703–710 (2000).
12. L. Zimmer, Y. Ikeda, R. Domann, and H. Yannis, "Simultaneous LIF and Mie scattering measurements for a branch-like spray cluster in an industrial oil burner," in AIAA Paper 02-0340 (AIAA, 2002), p. 1-1.
13. K. Kohse-Höinghaus, R. S. Barlow, M. Aldén, and J. Wolfrum, "Combustion at the focus: laser diagnostics and control," Proc. Combust. Inst. **30,** 89–123 (2005).
14. N. L. Smith, N. P. Megalos, G. J. Nathan, and D.-K. Zhang, "The significance of particle clustering in pulversied coal flames," Proc. Combust. Inst. **29,** 797–804 (2002).
15. H. Koh, J. Jeon, D. Kim, Y. Yoon, and J.-Y. Koo, "Analysis of signal attenuation for quantification of a planar imaging technique," Meas. Sci. Technol. **14,** 1829–1838 (2003).
16. M. C. Jermy, E. Berrocal, and F. Moukaideche, "Errors in light sheet images of polydisperse sprays: Monte Carlo simulation of photon propagation," in *12th International Symposium on Application of Laser Technology to Fluid Mechanics* (Calouste Gulbekian, 2004), paper 6.3.
17. M. C. Jermy, E. Berrocal, and F. Moukaideche, "Estimating the errors due to multiple scattering in spray imaging measurements: Experiments and simulation," in *ILASS-2004* (ILASS Europe, 2004), p. P12.
18. V. Sick and B. Stojkovic, "Attenaution effects on imaging diagnostics of hollow-cone sprays," Appl. Opt. **40,** 2435–2442 (2001).
19. D. G. Talley, J. F. Verdieck, S. W. Lee, V. G. Mcdonell, and G. S. Samuelsen, "Accounting for laser sheet extinction in applying PLLIF to sprays," in *34th Aerospace Sciences Meeting and Exhibit* (AIAA, 1996), pp. 96–469.
20. M. Versluis, N. Georgiev, L. Martisson, M. Aldén, and S. Kröll, "2-D absolute OH concentration profiles in atmospheric flames using planar LIF in a bi-directional laser beam configuration," Appl. Phys. B **65,** 411–417 (1997).
21. H. M. Hertz and M. Aldén, "Calibration of imaging laser-induced fluorescence measurements in highly absorbing flames," Appl. Phys. B **42,** 97–102 (1987).
22. R. Abu-Gharbieh, J. L. Persson, M. Försth, A. Rosén, A. Karlström, and T. Gustavsson, "Compensation method for attenuated planar laser images of optically dense sprays," Appl. Opt. **39,** 1260–1267 (2000).
23. P. A. M. Kalt and G. J. Nathan, "Corrections to facilitate planar imaging of particle concentration in particle-laden flow using Mie-scattering, Part 2: Diverging laser sheets," Appl. Opt. (submitted 2007).
24. A. Beer, *Einleitung in die höhere Optik* (Bonn, 1854).
25. J. H. Lambert, *Photometria* (Augsburg, 1760).
26. P. A. M. Kalt and C. H. Birzer, "Calibrations for planar nephelometry in densely-seeded two phase flows," in *Proceedings of the 4th Australian Conference on Laser Diagnostics in Fluid Mechanics and Combustion* (The University of Adelaide, 2005).
27. H. C. van de Hulst, *Light Scattering by Small Particles* (Wiley, 1957).
28. H. A. Becker, H. C. Hottel, and G. C. Williams, "On the light-scatter technique for the study of turbulence and mixing," J. Fluid Mech. **30,** 259–284 (1967).